ELSEVIER

Journal of Electron Spectroscopy and Related Phenomena 98–99 (1999) 245–256

JOURNAL OF ELECTRON SPECTROSCOPY and Related Phenomena

Properties and identification of oxygen sites at the $V_2O_5(010)$ surface: theoretical cluster studies and photoemission experiments

K. Hermann*, M. Witko☆, R. Druzinic, A. Chakrabarti, B. Tepper, M. Elsner, A. Gorschlüter, H. Kuhlenbeck, H.J. Freund

Fritz-Haber-Institut der MPG, Faradayweg 4-6, D-14195Berlin, Germany

Received 26 November 1997; accepted 18 March 1998

Abstract

Density functional theory cluster studies and angular resolved photoemission (ARUPS) measurements were performed to examine properties of differently coordinated surface oxygens at the $V_2O_5(010)$ surface. Calculations on embedded clusters as large as $V_{16}O_{49}H_{18}$ confirm the ionic character of the oxide. The computed width of the O 2sp dominated valence band region of V_2O_5 and the work function value of V_2O_5 (010) are in good agreement with the present photoemission data for freshly cleaved $V_2O_5(010)$ samples. Cluster derived total and partial densities of states (DOS, PDOS) can be used to identify differently coordinated surface oxygens. The PDOS referring to terminal (vanadyl) oxygens is localized near the center of the valence band whereas the PDOS's of the different bridging oxygens yield a broad distribution covering the full energy range of the valence bands. The shape of the experimental ARUPS curves for $V_2O_5(010)$ is well reproduced by the cluster DOS. Thus, the most prominent central peak in the experimental spectrum can be assigned to emission from terminal oxygen while the peripheral peaks at the top and bottom of the valence energy region are characterized as mixtures of vanadium with bridging oxygen induced contributions. This interpretation forms a basis to get insight into microscopic features at the real $V_2O_5(010)$ surface such as imperfections and adsorbate binding. The present study suggests that the different O 2sp derived peaks observed in the photoemission experiment may be taken as monitors of the differently coordinated oxygens at the oxide surface and can be used to study details of catalytic surface reactions in which these oxygens participate.

Keywords: Vanadium oxides; Photoemission; Density functional theory; Band structure; Clusters

1. Introduction

Vanadium oxides or vanadium containing systems are widely used as components of various catalysts in mild oxidation, ammoxidation, and dehydrogenation of hydrocarbons and other organic compounds. Further, they are efficient in oxidation of SO_2 to SO_3 and for the removal of NO_x by selective reduction with NH_3 [1,2]. The characteristic chemistry of vanadium based systems results from a number of different interrelated electronic and structural factors. This requires investigations by different experimental and theoretical techniques where a combination of theory and experiment can be particularly fruitful. As a first step towards an understanding of molecular mechanisms behind the above reactions at the catalyst surface, it is necessary to acquire a precise knowledge

* Corresponding author. Tel.: + 49-30-84134812; Fax: + 49-30-84134701; e-mail: hermann@fhi-berlin.mpg.de

☆ Permanent address: Institute of Catalysis and Surface Chemistry, Polish Academy of Sciences, ul. Niezapominajek, 30-239 Cracow, Poland

0368-2048/99/$ - see front matter
PII: S0368-2048(98)00290-4

of the geometrical and electronic surface structure itself. The crystal structure of divanadium pentoxide, V_2O_5, is rather complex and can be described in different ways. The orthorhombic crystal has a layer structure in which each layer consists of VO_5 subunits linked by edges (forming zig-zag rows) and by corners [3–5] with weak inter-layer coupling. The basal (010) and other non-basal planes differ in their bond type and in the degree of coordinative saturation of vanadium and oxygen atoms. This results in different behavior with respect to adsorption and catalytically supported reactions.

It is generally accepted that reactions of selective hydrocarbon oxidation at the catalytically active V_2O_5(010) surface proceed according to a redox mechanism where the hydrocarbon molecule loses one or two hydrogens and incorporates oxygen which originates from active sites of the oxide surface [1,2,6–8]. This process forms oxygen vacancies at the surface which may migrate into the bulk with the equivalent number of metal cations being simultaneously reduced. Gaseous oxygen participates in the oxidation reaction only after adsorption in other parts of the catalyst followed by migration through the lattice to the active site. The key point for understanding the mechanisms of selective hydrocarbon oxidation is to identify those structurally different surface oxygens which play the most important role in the reaction, i.e. which are responsible for abstraction of hydrogen(s) and which are inserted into the organic species yielding the oxygenated product. This issue has been discussed rather controversially in the literature. Some authors assume that terminal vanadyl oxygen (O=V) is removed from the catalyst surface to form a lattice vacancy [1] while others argue in favor of bridging oxygens (V–O–V or V–O–Me in the case of supported vanadia catalysts) and there are reports suggesting that a mixture of V=O and V–O–V(Me) type oxygens is essential for the selective oxidation process. However, the underlying mechanisms have not been verified by experiments on a microscopic basis, for an overview see Ref. [1].

Previous theoretical cluster studied using semiempirical [8–15] and ab initio methods (Hartree–Fock (HF) [16–18] and density functional theory (DFT) [19–21]) have shown consistently that two- and three-fold coordinated bridging oxygens can be removed more easily from the V_2O_5(010) surface than vanadyl oxygens. This result is confirmed by combined numerical (semiempirical HF) and experimental (IR) studies [22] on the importance of V_2O_5 surface oxygen for the oxidation of SO_2 into SO_3 which stress the preference of oxygen centers with the highest V coordination. Altogether, there is no experimental technique so far which can yield reliable microscopic information on the participation of differently coordinated surface oxygens in reactions at the V_2O_5 surface. This is also connected with the fact that a direct experimental identification of the different surface oxygens is very difficult if not impossible. Indirect information may be obtained from experimental techniques that probe the local electronic structure of surface oxygens since differently coordinated (and charged) oxygens are expected to result in different local electronic environments. In the present work we propose a combination of electronic structure calculations, based on cluster and periodic approaches, with experimental valence photoemission spectroscopy (ARUPS) to examine the O 2sp derived valence electron structure at the V_2O_5(010) surface. The theoretical results are consistent with experiment and suggest that the differently coordinated surface oxygens (terminal vanadyl oxygens, O(1), two- and three-fold coordinated bridging oxygens, O(2)/O(3)) make distinctly different contributions to the O 2sp valence density of states at the V_2O_5(010) surface. These contributions can be observed in the photoemission spectrum thus allowing an identification of the terminal and bridging surface oxygens by experiment. Therefore, changes in the photoemission spectrum induced by catalytically activated surface reactions may give information on the participation of differently coordinated surface oxygens.

In Section 2 we outline briefly the technical details of the theoretical and experimental methods used in the present work, while in Section 3 we present results and discussion. Finally, Section 4 summarizes our conclusions.

2. Technical details

2.1. Theoretical details

Divanadium pentoxide, V_2O_5, is characterized as a bulk material by a layer type orthorhombic structure

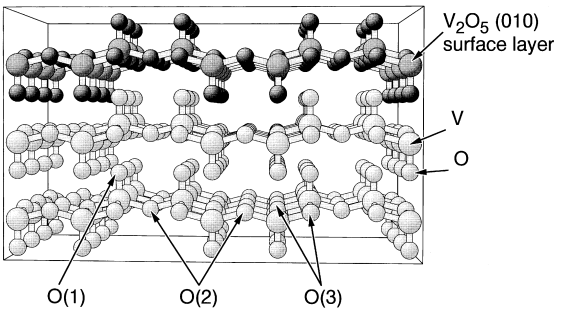

Fig. 1. Crystal structure of orthorhombic V_2O_5 with netplane stacking along (010). Vanadium (oxygen) centers are shown as large (small) balls. The atoms of a V_2O_5(010) single (surface) layer are emphasized by darker balls. Inequivalent oxygen centers, singly coordinated O(1), doubly coordinated O(2), triply coordinated O(3), are labelled accordingly.

[4,23,24] with layers extending parallel to the (010) net plane. Note that depending on the choice of the orthorhombic crystal axes the layer net plane orientation may also be denoted by (001) (interchanging lattice constants b and c), as, e.g., in Ref. [5], while we have adpoted an alternative nomenclature as used, e.g., in Ref. [25]. The layers are characterized by periodic arrangements of edge and corner sharing VO_5 pyramids sticking out at both sides of the layer, see Fig.1. There are three structurally different layer oxygens, terminal (vanadyl) oxygens O(1) coordinated to one vanadium atom through a short bond (d_{v-o} = 1.58 Å) and bridging oxygens O(2)/O(3) coordinated to two or three vanadiums with V–O

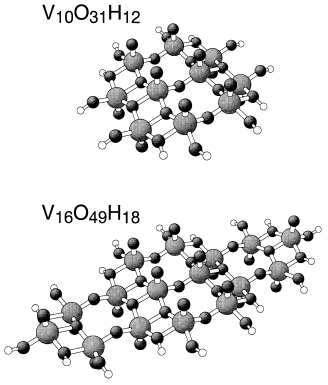

Fig. 2. Geometric structure of the $V_{10}O_{31}H_{12}$ and $V_{16}O_{49}H_{18}$ clusters used in the present calculations. The V(O) atoms are shown as large (small) shaded balls while very small while balls refer to hydrogen atoms used to saturate oxygen centers at the cluster boundary.

distances ranging between 1.78 Å and 2.01 Å. These oxygens represent five inequivalent centers at the ideal V_2O_5(010) surface (cf. Fig. 1): terminal (vanadyl) oxygens O(a) located directly above vanadium centers, oxygens O(b) bridging two vanadyl groups sticking out of the surface, oxygens O(c) bridging two vanadyl groups pointing into the bulk, and oxygens O(d, e) connecting three vanadyl groups of different surface orientation. In the present cluster calculations the local environment of the different oxygen sites is modeled by clusters $V_{10}O_{31}H_{12}$ and $V_{16}O_{49}H_{18}$ shown in Fig. 2 where all vanadium and oxygen positions are taken from the experimental bulk structure and peripheral oxygens are electronically saturated by hydrogen atoms [20]. The fixed substrate geometry is justified since the clusters are expected to simulate a local environment at the V_2O_5(010) surface rather than a finite (flexible) vanadium oxide cluster which is expected to assume a geometry quite different from that of a V_2O_5(010) surface. The periodic bulk (and single layer slab) calculations start from atom arrangements within the layers based on the experimental geometry [2,23,24] of the full 14 atom unit cell corresponding to two V_2O_5 units and lattice constants a = 11.519 Å, b = 4.373 Å, c = 3.564 Å. This geometry is further optimized in total energy minimizations to yield the theoretical equlibrium structure which is found to be very close to the experimental bulk structure [21].

The electronic structure of the clusters is determined by ab initio DFT where the Kohn–Sham orbitals are represented by linear combinations of atomic orbitals (LCAO's) using extended all-electron basis sets of contracted Gaussians from atom optimizations [26]. For the calculations the program package DeMon [27] is applied where electron exchange and correlation is approximated by the local spin density approximation (LSDA) based on the Vosko–Wilk–Nusair functional [28]. Detailed analyses of the electronic structure in the clusters are performed using Mulliken populations [29] and Mayer bond order indices [30,31]. Electronic states and optimized geometries of the periodic V_2O_5 bulk as well as of V_2O_5(010) oriented single layer slabs (in periodic slab geometry) are obtained by ab initio DFT calculations using the full-potential linear augmented plane wave (FLAPW) method [32,33]. In the periodic V_2O_5(010) slabs a vacuum region is introduced

Table 1
1. Atom charges from Mulliken analyses and Mayer bond orders for the $V_{10}O_{31}H_{12}$ and $V_{16}O_{49}H_{18}$ clusters. The charges Q refer to vanadium and oxygen atoms closest to the cluster center while P(O–V) denotes the bond orders between oxygen and its nearest vanadium neighbors. In addition, energies ϵ_{HOMO} of the highest occupied orbital and the valence energy width Δ in each cluster are given. For definitions see text.

	$V_{10}O_{31}O_{12}$	$V_{16}O_{49}H_{18}$
Q(V)	1.41	1.38
Q(O(1))	− 0.26	− 0.26
Q(O(2))	− 0.59	− 0.57
Q(O(3))	− 0.78	− 0.78
P(O(1)– V)	2.15	2.15
P(O(2)– V)	0.91/0.91	0.91/0.90
P(O(3)– V)	0.54/0.43/0.60	0.58/0.37/0.61
ϵHOMO (Ev)	− 7.07	− 7.09
Δ(eV)	5.40	5.64

between layers such that equivalent atoms to adjecent layers are separated by 10.933 Å (2.5*b) to suppress electronic inter-layer coupling. Further technical details of the present FLAPW calculations are given in Ref. [21].

2.2. Experimental details

Photoelectron data have been taken using a VSW ARIES spectrometer equipped with an electron analyzer rotatable in two orthogonal planes for angular resolved electron detection. A helium discharge lamp served as source for UV radiations. Most data presented here have been taken with HeII light (40.85 eV) incident at 45° with respect to the surface normal and the analyzer was set to detect electrons emitted normal to the surface. The pass energy of the analyzer was set to 15 eV which corresponds to a resolution of about 200 meV. In order to determine the work function, the high and low energy cutoffs of the spectra were recorded with HeI light (21.22 eV) using an analyzer pass energy of 1 eV. Here an acceleration voltage of − 5 V was applied to the sample since the slow electrons nearer to the low energy cutoff are very sensitive with respect to small electric and magnetic fields in the chamber. In addition, a reference spectrum of the metallic sample holder was taken to determine the high energy cutoff (Fermi level) of the spectra. This is necessary since V_2O_5 represents an insulating material which does not exhibit clearly visible intensity near the Fermi edge. The work function was determined by subtracting the width of the spectrum (high energy cutoff minus low energy cutoff) from the photon energy (21.22 eV).

The V_2O_5(010) samples have been prepared by in situ cleavage of V_2O_5 single crystals under UHV conditions. The crystals were not always perfectly ordered so that some cleavages led to strongly non-stoichiometric surfaces as was obvious from the photoelectron spectra. In these cases another cleavage was performed for the photoemission experiment. However, spectra taken from different surface samples exhibited always minor differences due to imperfections. All spectra presented in this work have been recorded at room temperature. Energy shifts due to charging effects have been observed only at temperatures below 150 K and can be excluded in the present study.

3. Results and discussion

In Table 1 the electronic structure of the present V_2O_5(010) surface clusters, $V_{10}O_{31}H_{12}$ and $V_{16}O_{49}H_{18}$, is characterized by atom charges (obtained from Mulliken population analyses) and Mayer bond order indices where the data refer to the central V and O atoms. As a first result we note that the calculated values are almost identical for the two clusters which indicates size convergence and shows that these clusters can be considered a realistic representation of the extended V_2O_5(010) surface. In agreement with chemical reasoning all vanadium atoms are positively charged and all oxygens negatively charged in the clusters. While the vanadiums are described by $V^{+1.40}$, singly coordinated terminal oxygens O(1) become $O^{-0.26}$, doubly coordinated bridging oxygens O(2) become $O^{-0.58}$, and triply coordinated bridging oxygens O(3) appear as $O^{-0.78}$. Hence, local charging of the different cluster atoms is found to be much smaller than formal valence charges, yielding V^{+5} and O^{-2}, would suggest. Obviously, interatomic binding in V_2O_5 is described by both ionic and sizeable covalent contributions. Further, negative charging of the oxygens increases monotonically with the coordination number which leads to charging being smallest for terminal O(1) and largest for triply coordinated bridging oxygens O(3). This indicates for

the V_2O_5(010) surface that bridging oxygen sites are more nucleophilic than terminal vanadyl sites which becomes important in view of the reactivity of the different sites with respect to surface chemical reactions. This conclusion can also be drawn from maps of the electrostatic potential $\Phi(r)$ for the two clusters [20,34] which yield negative minima above the bridging oxygens O(2) suggesting that electrophilic adparticles, like H^+, resulting from a surface reactions will be attracted preferentially at these sites and may form local surface bonds. A similar behavior was found in cluster studies for the MoO_3(010) and (100) surfaces [35,36].

Atom charges in the clusters can yield information about local ionicities and ionic (electrostatic) binding between the V and O atoms. In contrast, bond order results reflect local coordination and give a rough estimate of covalent contributions to the total V–O binding. The results of Table 1 confirm the general picture based on simple valence concepts. The bond order describing bonds between terminal (vanadyl) oxygens, O(1), and vanadiums yields values close to 2 which suggests V=O(1) double bonds and is consistent with the single coordination of these oxygens. Bond orders referring to binding between doubly coordinated bridging oxygens, O(2), and each of their two neighboring vanadiums result in values close to 1, corresponding to two single bonds per oxygen, which is again reasonable based on the coordination of O(2). Finally, V–O bond orders involving bridging atoms, O(3), coordinated to three vanadium neighbors each, give meaningful values of 0.5–0.6 per bond.

Table 1 contains also Kohn–Sham level energies ϵ_{HOMO} of the highest occupied orbitals (HOMO) of the $V_{10}O_{31}H_{12}$ and $V_{16}O_{49}H_{18}$ clusters. Based on general DFT theory [37] the quantity $-\epsilon_{HOMO}$ represents the first cluster ionization potential which will converge with increasing cluster size towards the work function of the V_2O_5(010) surface. In this spirit the calculated values $-\epsilon_{HOMO}$ represent a ''cluster work function'' of 7.1 eV which compares reasonably well with the experimental work function of V_2O_5(010) yielding 6.4 $\pm$ 0.7 eV in the present photoemission experiment and 6.7 $\pm$ 0.1 eV in vibrating capacitor measurements [38]. Note that the uncertainly of $\pm$ 0.7 eV mentioned before reflects local work function variations at the surface rather than an experimental error (amounting to 0.1 eV).

The electronic structure of the clusters can be characterized alternatively by energy level distributions of the occupied Kohn–Sham valence orbitals. These levels are dominantly O 2sp type with some V 3d admixture and are located between -12.47 (-12.73) eV and -7.07 (-7.09) eV for $V_{10}O_{31}H_{12}$ ($V_{16}O_{49}H_{18}$). This represents valence energy widths $\Delta =$ 5.4 and 5.6 eV respectively. An additional set of levels between -13.78 (-14.09) eV and -13.31 (-13.57) eV is due to split-off orbitals as a consequence of the bond saturation of peripheral oxygens by hydrogens in the clusters and therefore has to be considered a cluster artifact. The valence energy width Δ is expected to converge with increasing cluster size towards the total valence band width of the extended V_2O_5(010) surface system. Very recent FLAPW band structure calculations [21] yield for the V_2O_5 bulk $\Delta =$ 5.35 eV and for V_2O_5(010) single layer slabs $\Delta =$ 5.05 eV which is reasonably close to the cluster results suggesting again size convergence for the present clusters.

A full analysis of the electronic structure of the clusters requires a more detailed characterization of their valence orbitals The dense distribution of the O 2sp derived cluster levels in $V_{10}O_{31}H_{12}$ and $V_{16}O_{49}H_{18}$ allows the definition of a cluster total density of states (DOS) by

$$n_{tot}(\varepsilon) = \sum_k g(\alpha, \varepsilon - \varepsilon_k) \quad (1)$$

where $g(a\epsilon-\epsilon_k)$ denotes a Gaussian broadening function of width a centered at cluster level ϵ_k and the summation goes over all occupied cluster orbitals. Accordingly, atom projected partial densities of states (PDOS) can be determined using orbital populations by

$$n_A(\varepsilon) = \sum_k q_k(A) g(\alpha, \varepsilon - \varepsilon_k) \quad (2)$$

where $q_k(A)$ gives the population of atom A in cluster orbital ψ_k determined by a Mulliken analysis. Due to the additivity of Mulliken populations the total DOS can be decomposed into its atom projected contributions by

$$n_{tot}(\varepsilon) = \sum_A n_A(\varepsilon). \quad (3)$$

Fig. 3 shows the total and atom projected DOS

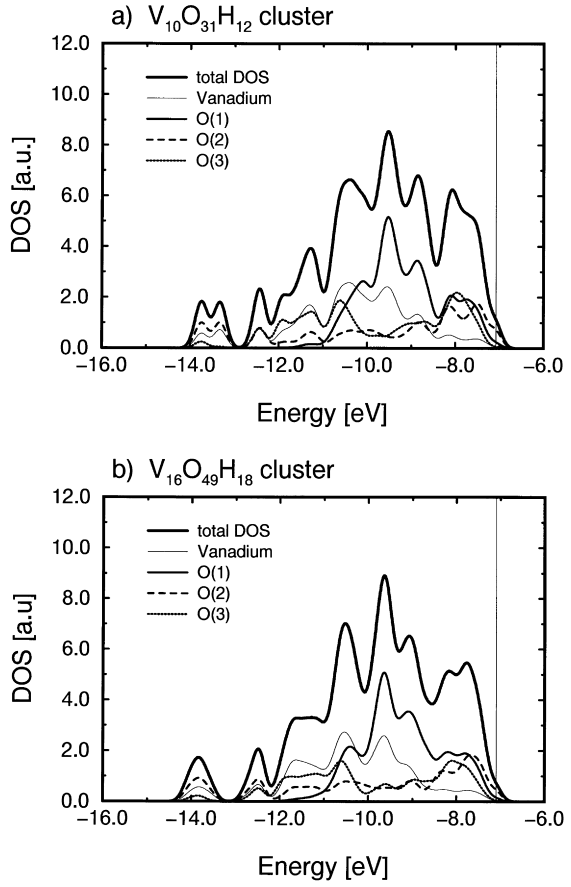

Fig. 3. Total and atom projected DOS for the clusters $V_{10}O_{31}H_{12}$ (a) and $V_{16}O_{49}H_{18}$ (b), see text. The results refer to a Gaussian level broadening of 0.4 eV (FWHM) and the HOMO energy is marked by a thin vertical line.

curves for the clusters $V_{10}O_{31}H_{12}$ (Fig. 3a) and $V_{16}O_{49}H_{18}$ (Fig. 3b) where the vanadium contributions as well as those from all differently coordinated oxygens O(1), O(2), O(3), are included and a Gaussian level broadening of 0.4 eV (FWHM) is applied. Despite the different sizes of the two clusters the overall shapes of the DOS curves of Fig. 3a and b are very similar and can be discussed jointly. The total DOS in the energy region between − 13 and − 7 eV (denoted valence region in the following) shows a multi-peak structure described by dominantly O 2sp derived electron states without noticeable energetic separation between O 2s and O 2p and by V 3d contributions as mentioned above. (Note that the DOSs in Fig. 3 do not exhibit a sharp cut-off at the

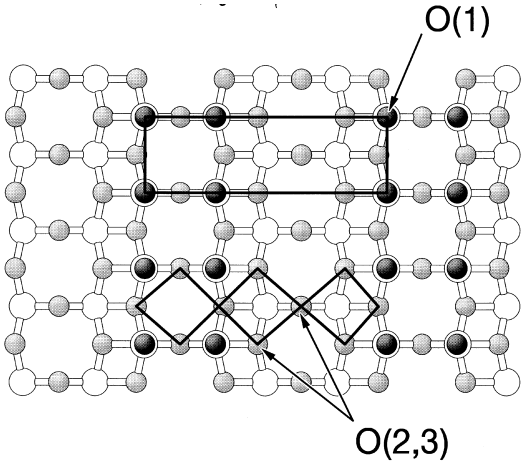

Fig. 4. Geometric structure of a V_2O_5(010) single layer emphasizing the oxygen sub-lattices: wide lattice of terminal O(1) (dark shaded balls), dense lattice of bridging O(2,3) (light shaded balls). Vanadium atoms are shown as white spheres.

HOMO energy (− 7.07 eV, marked by thin lines in the plots) which is due to the Gaussian broadening.) The additional DOS peaks close to −14 eV reflect the split-off energy levels arising from bond saturation of peripheral cluster oxygens discussed before and can be neglected for the present purpose.

The vanadium projected partial densities of states of Fig. 3 show moderate variations with larger values near the central part of the valence region. The sizes of these metal derived PDOS are smaller compared to those of all oxygens but are not negligible. An integration over the valence region yields populations of 3.6 electrons per V atom in agreement with the population data of Table 1. As a result, the V atoms in the clusters are not fully ionic according to their formal valence charge (V^{+5}) and covalent contributions become important for the interatomic V–O binding. The partial densities of states referring to the terminal (vanadyl) oxygens O(1) are, in both clusters, concentrated near the center of the valence region with smaller contributions above the center and they are described by an overall more confined (∼ 3 eV wide) distribution compared to that of the total DOS of the valence region. In contrast, the PDOSs of the bridging oxygens O(2,3) yield a broad distribution covering the full energy range of the total DOS (∼5.5 eV). Obviously, the O(1) derived cluster levels show a dispersion width which is smaller than to that

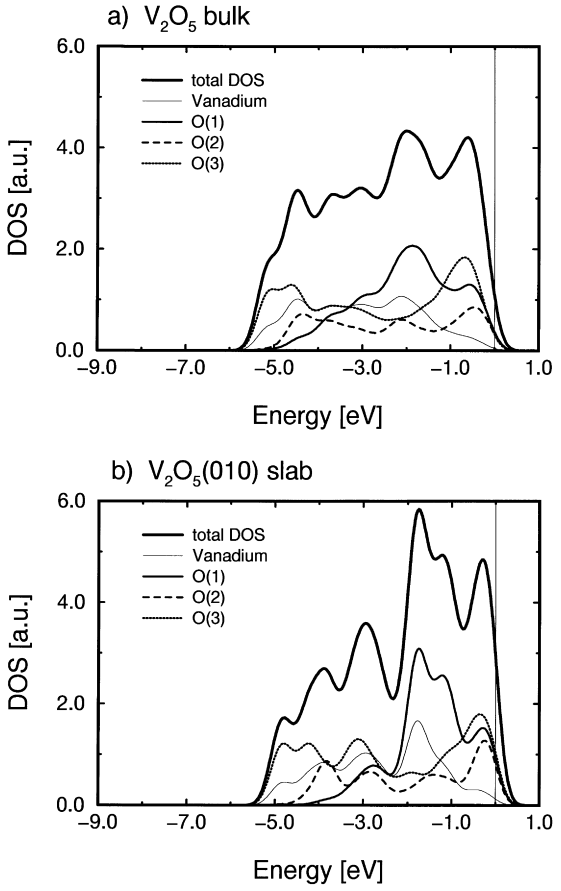

Fig. 5. Total and atom projected DOS for the V_2O_5 bulk (a) and V_2O_5(010) single layer slab (b), see text. The results refer to a Gaussian broadening of 0.5 eV (FWHM). The top of the valence band is marked by a thin vertical line and defines the energy zero.

of bridging O(2,3) species. This is partly due to the spatial distribution of the different oxygens in the crystal. Fig. 4 displays the geometric structure of a V_2O_5(010) single layer where the terminal oxygens, O(1), are represented by dark shaded balls while the two- and three-fold coordinated bridging oxygens, O(2,3), are shown as light balls and vanadiums are sketched as white spheres. The average interatomic distance between terminal O(1) is larger and there are fewer terminal oxygens inside the lateral unit area (sketched by the black rectangle in Fig. 4) compared to the arrangement of the bridging oxygens. As a result, the effective interatomic interaction within the O(1) sub-lattice is weaker than that within the O(2,3) sub-lattice which, in a simple tight-binding picture, translates to different dispersion widths found for the two oxygen sub-lattices. However, this simple geometric can serve only as a crude guideline since electronic coupling between the two oxygen sublattices, both direct and via V atoms, is neglected. A more detailed description of the oxygen derived electronic structure inside the V_2O_5(010) layers must account for hybridization effects between the sublattices which introduces additional PDOS broadening and shifts and makes the above interpretation only qualitatively meaningful. The energy distribution of the oxygen derived states and PDOSs is influenced by both covalent and ionic coupling. As shown by the population analyses, cf. Table 1, the negative charges on the differently coordinated oxygens differ somewhat (with the terminal oxygens exhibiting the smallest charge). As a consequence, one may expect electrostatic shifts acting on the respective O 2sp orbital energies which distinguish between the different oxygens. However, this shifting is combined with dispersion effects due to covalent coupling and cannot be considered separately.

Fig. 5 shows total and atom projected DOS curves from FLAPW band structure calculations for the V_2O_5 bulk (Fig. 5a) and V_2O_5(010) single layer slabs (in repeated slab geometry, Fig. 5b). The computed curves have been smoothed by a Gaussian broadening of 0.5 eV (FWHM) and the energy scale has been shifted to yield an energy $\epsilon_0 = 0$ for the upper valence band edge. (In analogy to the cluster result the DOSs do not show a sharp cut-off at the e_0 as a result of Gaussian broadening.) Further, the PDOS curves are obtained by (Eq. 2) where weighing factors $q_k(A)$ are determined by respective atom charges inside inequivalent muffin tin spheres of the unit cells [21]. A comparison of the DOSs from the bulk and slab calculations with those for the present clusters shows rather similar behavior. The multi-peak structure extending over an energy range of 5.5 eV are characterized by dominantly O 2sp derived electron states with V 3d contributions analogous to the cluster results.

The partial densities of states due to the terminal oxygens O(1) are, for both the bulk and the single layer slab, concentrated near the center of the valence region with smaller contributions above the center. Further, these PDOSs extend over an energy region of only ~ 3 eV compared to a width of 5.5 eV of the

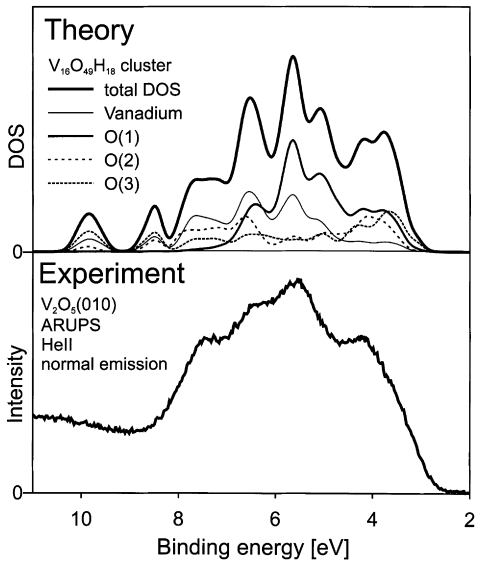

Fig. 6. Comparison of the total and atom projected density of states calculated for a $V_{16}O_{49}H_{18}$ cluster with a photoelectron spectrum (HeII light, normal emission).

total valence DOS of the valence region. This contrasts with the PDOSs of the bridging oxygens O(2,3) which yield a broad distribution over the full energy range of the total DOS. The difference between the O(1) and O(2,3) derived PDOSs can be explained by the same arguments as given for the cluster PDOSs. The average interatomic distance between terminal oxygens O(1) is larger than that of the bridging oxygens O(2,3) which yields a smaller effective interatomic interaction and hence smaller dispersion width for O(1) compared with that for O(2,3). A more detailed comparison shows that the O(1) derived PDOS differs more strongly between the V_2O_5 bulk and the V_2O_5(010) single layer slab than those of the O(2,3). This is due to a simple geometric effect. The terminal oxygens O(1) stick out of the V_2O_5(010) layers and will be influenced most by the inter-layer coupling in the bulk as opposed to the bridging oxygens O(2,3) which reside well inside the layers. Thus, the missing inter-layer coupling in the isolated single layers affects the O(1) more strongly than the O(2,3) species.

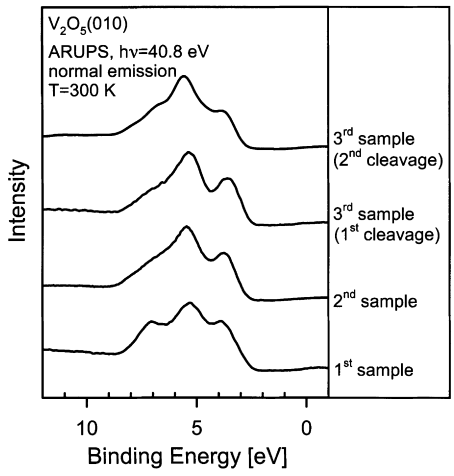

Fig. 7. Angular resolved photoemission spectra (ARUPS) of V_2O_5(010). The spectra have been recorded for different samples directly after cleavage (HeII light, normal emission).

A comparison of the V_2O_5(010) single layer DOS (Fig. 5b) with that of the largest cluster $V_{16}O_{49}H_{18}$ (Fig. 3b) yields a very similar peak structure as mentioned before. The relative weights of the different peaks change somewhat between the single layer and the cluster which reflects the geometric differences between the two systems. A comparison of the PDOSs reveals also qualitative similarities. However, a more detailed quantitative analysis is difficult since the PDOS definitions are somewhat different in the band structure methods (projections based on charges inside atom spheres) and in cluster calculations (projections based on population analyses). Altogether, the qualitative similarity between the DOS results for the V_2O_5 bulk, the V_2O_5(010) single layer slab, and the V_2O_5 surface clusters indicates that the different approaches yield basically the same electronic structure of the oxide material and can therefore be applied alternatively to model bulk and surface properties.

Fig. 6 shows an ARUPS spectrum for V_2O_5 taken with HeII light in normal emission geometry together with DOS and PDOS curves calculated for the $V_{16}O_{49}H_{18}$ cluster, cf. Fig. 3b, where the energy scale of the theoretical data is shifted appropriately. Obviously, the shape of the experimental intensity is well reproduced by the calculated total DOS. This suggests that the origin of peaks observed in the photoemission spectrum may be identified by a comparison with the calculated PDOSs. As a result, the most prominent peak in the experimental data is to be assigned mainly to emission from terminal oxygen, O(1), while the peak at a binding energy of about 7 eV

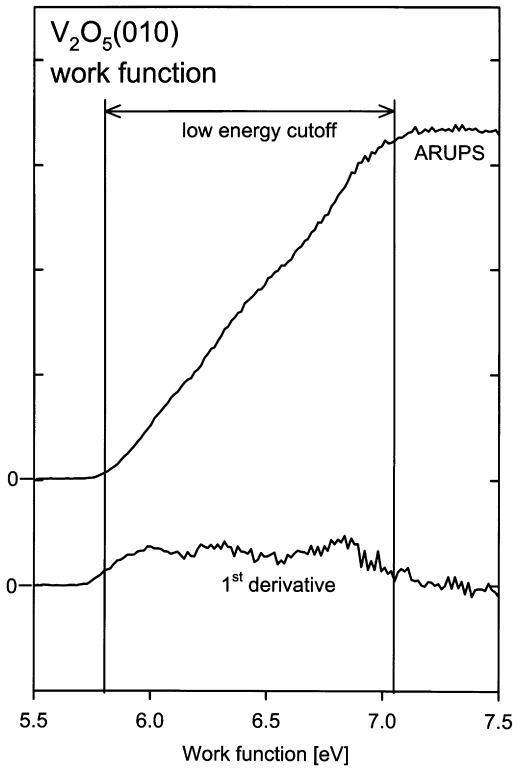

Fig. 8. Low energy cutoff of a photoelectron spectrum of V_2O_5(010) taken with HeI light at normal emission (top curve). The energy scale has been shifted to relflect work function values. The bottom curve gives the first derivative of the cutoff spectrum.

is to be characterized as a mixture of vanadium with O(2) and O(3) induced intensity. The feature at about 4 eV is interpreted as emission from all three types of surface oxygen which contribute similar amounts.

As noted in the introduction, results of previous cluster model studied on V_2O_5(010) [8–21] have indicated that the singly coordinated vanadyl oxygens, O(1), are more strongly bound to the surface than bridging oxygens, O(2,3). This is consistent with the present experimental data concerning surface imperfections. Fig. 7 shows a set of ARUPS curves which are taken from different V_2O_5(010) surface samples obtained by several cleavages. Obviously, the spectra vary somewhat with differences showing up most prominently in the peak at about 7 eV binding energy. In contrast, the dominant feature at about 5.5 eV, which is interpreted as mainly due to emission from O(1) surface oxygens, is much less influenced. Therefore, the ARUPS data suggest that the concentration of surface imperfections involving the O(1) species changes only little between different cleavages. This can be understood by the vanadyl oxygens being more strongly bound to the surface than bridging oxygens. As a consequence, the more weakly bound bridging oxygens contribute more to surface imperfections reflected in the differences between the spectra. Scanning tunneling microscopy (STM) images reported in literature [39] reveal the different areas of a freshly cleaved V_2O_5(010) surface exhibit different contrasts. Based on image simulations the authors attribute this result to incomplete and inhomogeneous occupation of vanadyl oxygen sites. However, following the above ARUPS interpretation the present results do not support the conclusion from the STM analysis but, instead, favor incomplete occupation of bridging oxygen sites.

Imperfections of the V_2O_5(010) surface show up also in the low energy cutoff of the photoelectron data. For perfectly homogeneous surfaces this cutoff is expected to be a vertical line broadened only by experimental resolution and thermal effects which indicates that all parts on the surface under inspection are characterized by the same work function. Surface imperfections introduce different local work function values in different parts of the surface which broadens the cutoff. As an example, Fig. 8 shows in the upper part the low energy cutoff from the present ARUPS data for a cleaved V_2O_5(010) sample where the energy scale has been shifted to reflect work function values. The broad cutoff region which is evident from this figure yields a range of local work functions at the sample surface which extends from about 5.8 to 7.1 eV indicating clearly an inhomogeneous surface in agreement with previous STM results [39]. Fig. 8 includes at the bottom the first derivative of the cutoff spectrum. This curve exhibits three weak peaks at 6.0, 6.3, and 6.8 eV which may be viewed as an indication of three different types of imperfection structures. However, a definitive characterization of possible imperfection structures requires a much more detailed analysis which goes beyond the present study.

Fig. 9 shows ARUPS data for V_2O_5(010) exposed to different doses of hydrogen (H_2) where the spectra have been taken with HeII light in normal emission. As expected, the spectra are found to vary with increasing dosage which is attributed to hydrogen

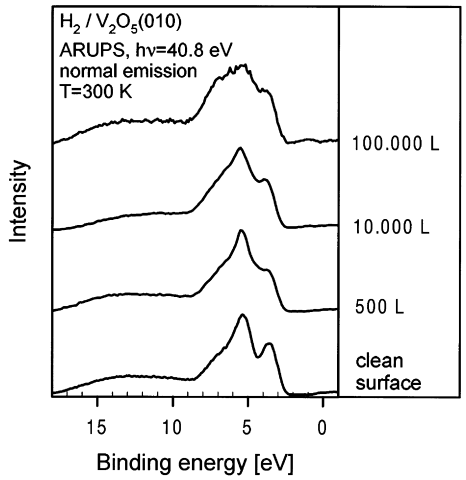

Fig. 9. Angular resolved photoemission spectra (ARUPS) of V_2O_5(010) for different doses of hydrogen (H_2) indicated in the figure. The spectra have been recorded with HeII light for normal electron emission

reacting with the surface. Interestingly, the differences with coverage are most pronounced in the peripheral features at 3.5 and 7 eV binding energy while the intensity of the dominant peak at about 5.5 eV seems to be affected only little. Based on the present interpretation of the different photoemission peaks the data of Fig. 9 suggest that reacting hydrogen affects bridging surface oxygens more strongly than terminal vanadyl oxygens. Since bridging oxygens are more weakly bound to the surface than terminal oxygens the former are more likely to react with the absorbing hydrogen to create surface oxygen vacancies. This is consistent with theoretical results [16–19] indicating that surface OH which may be formed as a reaction intermediate at the V_2O_5(010) surface is more mobile at bridging than at terminal oxygen sites.

4. Conclusions

The present combined theoretical and experimental study can provide detailed information on the electronic structure of the V_2O_5(010) surface. This applies in particular to the behavior of differently coordinated surface oxygens which can participate in catalytically activated reactions surface at the vanadium oxide surface. The electronic parameters calculated for the present cluster models, $V_{10}O_{31}H_{12}$ and $V_{16}O_{49}H_{18}$ are size converged and, therefore, the clusters can be considered realistic models of the extended V_2O_5(010) surface. The theoretical results confirm the ionic character of the material where, however, major covalent contributions participate in the V–O binding and distinguish between the differently coordinated oxygen sites. Both the width of the O 2sp dominated valence band region and the work function determined from the cluster models are in good agreement with the angular resolved photoemission data for freshly cleaved V_2O_5(010) samples presented in this study. Further, total and atom projected partial densities of states have been determined from Kohn–Sham levels and orbitals of the clusters. An analysis of the total DOS confirms that dominant O 2sp character of the valence energy region with some V 3d contributions and the PDOSs can be used to identify differently coordinated oxygens. The PDOS referring to the terminal (vanadyl) oxygens O(1), is localized near the center of the valence energy region whereas the PDOSs of the bridging oxygens, O(2,3), yield a broad distribution covering the full energy range of the total DOS. The different behavior can be understood by the spatial distribution of oxygens in the different oxygen sublattices and the size of their nearest neighbor coupling. This is consistent with results from FLAPW band structure calculations for the periodic V_2O_5 bulk and V_2O_5(010) single layer slabs [21] where the overall shapes of the total and atom projected DOS curves are in good agreement with the cluster results.

Further, angular resolved photoemission spectra have been measured for freshly cleaved V_2O_5(010) surface samples. The shape of the experimental spectra in the valence energy region is well reproduced by the calculated total DOS of the present clusters. This suggests that the origin of peaks observed in the photoemission spectrum may be identified by a comparison with the calculated cluster PDOSs. Thus, the most prominent peak in the experimental spectrum can be assigned mainly to emission from terminal oxygen, O(1), while the peripheral peaks at the top and bottom of the valence energy region are characterized as mixtures of vanadium with O(2) and O(3) induced contributions. This interpretation forms a basis to get insight into microscopic features at the real V_2O_5(010) surface. First, the variation of ARUPS curves for different V_2O_5(010) samples, cf. Fig. 7,

affects the peripheral peaks more than the dominant central peak which suggests that imperfections introduced by surface oxygen vacancies refer to bridging rather than terminal vanadyl species. This is consistent with results of previous cluster studies [8–21] which suggest that vanadyl oxygens are more strongly bound to the surface than bridging oxygens. Second, ARUPS measurements for V_2O_5(010) exposed to different doses of hydrogen (H_2) yield spectra which vary with increasing coverage, cf. Fig. 9, where the differences with coverage are most pronounced in the peripheral peaks. This suggests that adsorbing hydrogen affects bridging surface oxygens more strongly than terminal vanadyl oxygens. Since bridging oxygens are more weakly bound to the surface than terminal oxygens the former are more likely to react with the absorbing hydrogen to create surface oxygen vacancies. This is consistent with results from recent cluster studies [16–19] which suggest that surface OH which may be formed as a reaction intermediate at the V_2O_5(010) surface is more mobile at bridging than at terminal oxygen sites. Altogether, the present study confirms that the combination of photoemission experiments and electronic structure calculations can add to the detailed microscopic understanding of complex transition metal oxide surfaces. Moreover, the present theory suggest that the different O 2sp derived peaks observed in the photoemission experiment may be taken as monitors of the differently coordinated surface oxygens and can be used to study details of catalytic reactions at the oxide surface where oxygens participate.

Acknowledgements

This work has been supported in parts by Deutsche Forschungsgemeinschaft and by Fonds der Chemischen Industrie. We thank Prof. S. Horn (University of Augsburg) for providing us with V_2O_5 single crystals.

References

[1] B. Grzybowska-Swierkosz, F. Trifiro, J.C. Vedrine, Eds., Vanadia Catalysts for Selective Oxidation of Hydrocarbons and Their Derivatives, J. Appl. Catal., 157 (1997) 1-420.
[2] B. Grzybowska-Swierkosz, J. Haber (Eds.), Vanadia Catalysts for Processes of Oxidation of Aromatic Hydrocarbons PWN–Polish Scientific Publishers, Warsaw, 1984.
[3] A. Byström, K.A. Wilhelmi, O. Brotzen, Acta Chem. Scand. 4 (1950) 1119.
[4] H.G. Bachman, F.R. Ahmed, W.H. Barnes, Z. Kristallogr. Kristallgeon. Kristallphys.Kristallchem. 115 (1981) 110.
[5] R.W.G. Wyckoff, Crystal Structures, Interscience Publishers, John Wiley & Sons, Inc,, New York, London, Sydney, 1965.
[6] A. Bielanski, J. Haber, Oxygen in Catalysis, Marcel Dekker Inc, New York, 1990.
[7] A. Bielanski, J. Piwowarczyk, J. Pozniczek, J. Catal. 113 (1988) 334.
[8] J. Haber, M. Witko, R. Tokarz, J. Appl. Catal. 157 (1997) 3.
[9] M. Witko, R. Tokarz, J. Haber, J. Mol. Catal. 66 (1991) 205.
[10] M. Witko, R. Tokarz, J. Haber, J. Mol. Catal. 66 (1991) 357.
[11] M. Witko, Catal. Today 32 (1996) 89.
[12] M. Witko, R. Tokarz, J. Haber, J. Appl. Catalysis A 157 (1997) 23.
[13] R.F. Nalewajski, J. Korchowiec, R. Tokarz, E. Broclawik, M. Witko, J. Mol. Catal. 77 (1992) 165.
[14] R.F. Nalewajski, J. Korchowiec, J. Mol. Catal. 82 (1993) 383.
[15] M. Witko, R. Tokarz, K. Hermann, Polish J. Chem. 72 (1998) 15.
[16] M. Witko, K. Hermann, J. Mol. Catal. 81 (1993) 279.
[17] M. Witko, K. Hermann, in Studies in Surface Science and Catalysis, S.V. Bellon, V.C. Corberan, Eds., Vol. 82 (1994), p. 94.
[18] M. Witko, K. Hermann, R. Tokarz, J. Electr. Spectr. and Rel. Phen. 69 (1994) 89.
[19] K. Hermann, A. Michalak, M. Witko, Catal. Today 32 (1996) 321.
[20] A. Michalak, M. Witko, K. Hermann, Surf. Sci. 375 (1997) 385.
[21] A. Chakrabarti, K. Hermann, R. Druzinic, M. Witko, F. Wagner, M. Petersen, Phys. Rev. B, in print.
[22] R. Ramirez, B. Casal, L. Utrera, E. Ruiz-Hitzky, J. Phys. Chem. 94 (1990) 8960.
[23] L. Kihlborg, Arkiv Kemi 21 (1963) 357.
[24] H. Hanke, R. Bunert, H.G. Jetschewitz, Z. Anorg. Allg. Chem. 109 (1975) 414.
[25] R. Ramirez, B. Casal, L. Utrera, E. Ruiz-Hitzky, J. Phys. Chem. 94 (1990) 8960.
[26] N. Godbout, D. R. Salahub, J. Andzelm, E. Wimmer, Can. J. Phys. 70 (1992) 560.
[27] The DFT-LCGTO program package DeMon was developed by A. St.-Amant and D. Salahub (University of Montreal). Here a modified version with extensions by A. Michalak and L.G.M. Petterson is used.
[28] S.H. Vosko, L. Wilk, M. Nusair, Can. J. Phys. 58 (1980) 1200.
[29] R.S. Mulliken, J. Chem. Phys., 23 (1955) 1833, 1841, 2388, 2343.
[30] I. Mayer, Chem. Phys. Lett. 97 (1983) 270.
[31] I. Mayer, J. Mol. Struct. (Theochem) 149 (1987) 81.
[32] P. Blaha, K. Schwarz, P. Sorantin, S.B. Trickey, Comput. Phys. Commun. 59 (1990) 399.
[33] B. Kohler, S. Wilke, M. Scheffler, R. Kouba, C. Ambrosch-Draxl, Comput. Phys. Commun. 94 (1996) 31.

[34] M. Witko, K. Hermann, R. Tokarz, Catal. Today, submitted.
[35] A. Michalak, K. Hermann, M. Witko, Surf. Sci. 366 (1996) 323.
[36] K. Hermann, M. Witko, A. Michalak, Catal. Today, submitted.
[37] J.K. Labanowski, J.W. Anzelm (Eds.), Density Functional Methods in Chemistry Springer-Verlag, New York, 1991.
[38] G. Grymonprez, L. Fiermans, J. Vennik, Surf. Sci. 36 (1973) 370.
[39] R.L. Smith, W. Lu, G. S Rohrer, Surf. Sci. 332 (1995) 293.